Segregation and wetting transition at dislocations

Article *in* Metallurgical and Materials Transactions A · January 2006

DOI: 10.1007/s11661-006-0119-6

CITATIONS
10

READS
35

4 authors, including:

Nanyu Ma
Shandong University
14 PUBLICATIONS **452** CITATIONS
SEE PROFILE

Chuan-Chou Shen
National Taiwan University
413 PUBLICATIONS **10,519** CITATIONS
SEE PROFILE

Yunzhi Wang
The Ohio State University
328 PUBLICATIONS **7,835** CITATIONS
SEE PROFILE

Segregation and Wetting Transition at Dislocations

N. MA, C. SHEN, S.A. DREGIA, and Y. WANG

We investigate solute segregation and wetting transition at dislocations and the corresponding drag effect on dislocation glide using a continuum model developed previously for grain boundary and based on gradient thermodynamics. The dislocation core structure and stress field are described by the newly developed phase field model. This study differs from much previous work because it takes into account not only the long-range elastic interactions but the short-range chemical interactions between solute atoms and dislocation core as well as among solute atoms themselves. The latter leads to the prediction of a wetting transition at the dislocation core with respect to varying temperature, solute concentration, or dislocation velocity. The transition temperatures obtained during heating and cooling are different from each other, leading to a hysteresis loop in the solute concentration-temperature plot and the solute concentration-velocity plot. These predictions could provide new insights into the phenomena of sharp yield point drop and strain aging observed in metal alloys.

I. INTRODUCTION

SEGREGATION and clustering of solutes at extended crystalline defects such as surfaces, grain boundaries, heterophase interfaces, and dislocations play a key role in microstructural evolution and plastic deformation of alloys during their thermal and mechanical processing (for reviews, see the monographs by Sutton and Balluffi[1] and Hirth and Lothe[2]). The chemical equilibrium of a system of extended defects is characterized by gradient thermodynamics[3–9] and its discrete counterpart (discrete lattice model).[10,11,12] Hillert[11,12] pioneered the use of a regular solution model in nonuniform systems, which was later applied extensively to treat solute segregation at surfaces and interfaces.[13–19] In this article, we use the continuum model developed by Ma *et al.*[20] for grain boundary segregation based on gradient thermodynamics and the phase field model of dislocations developed by Wang *et al.*[21,22] and Shen *et al.*[23,24] to investigate solute segregation and wetting transition at dislocations and the corresponding drag force on dislocation glide.

The problem of solute segregation at dislocations was first analyzed by Cottrell.[25] Later, the treatment was refined by a number of authors.[2,26–32] It was found that solute atoms are drawn toward or away from dislocations as a result of the interactions of their strain fields, leading to solute-rich and solute-lean regions around the dislocations called the Cottrell atmosphere. The solute atoms may move together with the dislocations, imposing a drag force on them, or break away from them, depending on the interplay between the characteristic time scales of solute atom diffusion and dislocation motion. At relatively high temperatures and low rates of strain, the solute atoms may repeatedly segregate at and break away from the dislocations, resulting in a repeated yielding. Such an effect is believed to be responsible for the serrations in the stress-strain curve and is often referred to as the Portevin-LeChatelier (PLC) effect.[33]

Most of these studies have focused primarily on the long-range elastic solute-dislocation interactions and ignored the short-range chemical (or inelastic) interactions by considering ideal or dilute solutions. If there is a strong interaction between the solute atoms and the extended defects, solute-rich atmospheres around the defects cannot be treated as dilute solution anymore, irrespective of how dilute the bulk concentration is, and the solute-solute interaction has to be considered. Conversely, if the level of segregation is high, large concentration gradients exist near the defects and their contributions to the chemical potential (including coherency strain energy) must be included in the condition for equilibrium. In a recent study on impurity segregation at grain boundaries,[20] it was shown that the consideration of solute-solute interactions results in a first-order segregation transition at grain boundaries, leading to a sharp transition of grain boundary mobility as a function of temperature. Similar effects are expected for impurity segregation at other defects and have been demonstrated for solute-dislocation interactions.[34] Although the early models are convenient for illustrating the basic characteristics of solute segregation at dislocations and their effect on dislocation glide, more robust solution thermodynamics and solute-dislocation core interaction models are needed for capturing more sophisticated phenomena observed in experiments. In this study, we consider contributions to the chemical equilibrium from concentration gradient and structural discontinuity. In contrast to most previous studies, our model includes several distinct terms accounting for the short-range chemical interactions, concentration gradient, coherence elastic strain, and spatial variation of the gradient-energy coefficient as well as the enthalpy of mixing near a dislocation. The model is applied to study (1) segregation profiles at stationary and steady-state gliding straight dislocations; (2) drag forces at the gliding dislocations; and (3) wetting transitions with respect to solute concentration, temperature, and dislocation velocity.

This study could serve as a preliminary step in applying the widely used phase field method to study impurity

N. MA, Postdoctoral Candidate, C. SHEN, Postdoctoral Candidate, S.A. DREGIA, Associate Professor, and Y. WANG, Associate Professor, are with the Department of Materials Science and Engineering, The Ohio State University, 2041 College Road, Columbus, OH 43210. Contact e-mail: wang.363@osu.edu

This article is based on a presentation made in the ''Hillert Symposium on Thermodynamics & Kinetics of Migrating Interfaces in Steels and Other Complex Alloys,'' December 2–3, 2004, organized by The Royal Institute of Technology in Stockholm, Sweden.

segregation at dislocations of complicated configurations. Using gradient thermodynamics and field description of structural and chemical nonuniformities, the phase field method can, in principle, describe microstructural evolution in nonuniform systems consisting of many types of defects, such as homo- and heterophase interfaces, antiphase domain boundaries, ferromagnetic and ferroelectric domain walls, dislocations, and microcracks, to name a few. Because analytical treatments are limited to simple configurations, there is an increasing interest in applying computer simulation techniques to study various phenomena that involve solute-dislocation interactions, including clustering of solutes around dislocations,[34–37] dislocation migration in the presence of solutes,[34,36,38,39] stress-assisted nucleation in the vicinity of dislocations,[40–43] and collective dislocation-impurity interactions (*e.g.,* dynamic strain-aging).[44,45] The recent advances in the phase field approach to dislocation plasticity[21–24,37,39] provide an opportunity for simulating the effects of solute-dislocation interaction on the evolution of a population of dislocations of arbitrary configurations such as dislocation substructures.

II. THEORETICAL FORMULATION

A. *Segregation Model*

As mentioned previously, the study of solute segregation at extended defects requires the consideration of contributions to the chemical potential from structural and chemical nonuniformities. For segregation at dislocations considered in this study, we follow the segregation model developed recently for grain boundary[20] in a binary substitutional alloy to account for the solute-dislocation and solute-solute interactions. In this approach, the chemical potential of solute atoms in a chemically homogeneous but structurally nonuniform (incoherent or defective) system is expressed as

$$\bar{\mu}_B(\mathbf{r}) = \bar{\mu}_B^0(\mathbf{r}) + k_{\mathrm{B}}T\ln c + \bar{\mu}_B^{xs}(\mathbf{r},c) \qquad [1]$$

where $\mathbf{r}$ is an arbitrary point in the system, k_B is Boltzmann's constant, T is temperature, $\bar{\mu}_B^0$ is the standard-state value (*i.e.,* a state of pure B in the presence of structural defects at a pressure of 1 atm), and $\bar{\mu}_B^{xs}$ is the part in excess of the contribution from configurational entropy of mixing. If the structural nonuniformity is associated with dislocations, the variation of the standard-state value with position can be expressed as

$$\bar{\mu}_B^0(\mathbf{r}) = \bar{\mu}_B^0(\infty) + U_B^{ch}(\mathbf{r}) + U_B^{el}(\mathbf{r}) \qquad [2]$$

where ∞ represents a point far away from the dislocations and $U_B^{ch}(\mathbf{r})$ and $U_B^{el}(\mathbf{r})$ are, respectively, the short-range chemical and long-range elastic interaction potentials between solute atoms and dislocations. $U_B^{ch}(\mathbf{r})$ is associated with the variation in coordination number of atoms at the dislocation core and is therefore confined within the core region. It may translate with the dislocations but is not otherwise altered in shape or amplitude. $U_B^{el}(\mathbf{r})$ is associated with lattice distortion caused by the dislocations and therefore depends on the dislocation configuration. Correspondingly, the ''excess'' chemical potential is expressed as

$$\bar{\mu}_B^{xs}(\mathbf{r},c) = \bar{\mu}_B^{xs}(\infty,c) + \varphi_B(\mathbf{r},c) \qquad [3]$$

where $\varphi_B(\mathbf{r},c)$ takes into account the position dependence of the enthalpy of mixing near a dislocation because of the variation in coordination number. The difference in solute chemical potentials near a dislocation and far away from it can then be expressed as

$$\bar{\mu}_B - \bar{\mu}_B^{\infty} = U_B^{ch}(\mathbf{r}) + U_B^{el}(\mathbf{r}) + \varphi_B(\mathbf{r},c) + k_BT\ln(c/c_\infty) + [\bar{\mu}_B^{xs}(\infty,c) - \bar{\mu}_B^{xs}(\infty,c_\infty)] \qquad [4]$$

For a chemically nonuniform system, the exchange potential includes contributions from the concentration gradient and the associated coherency elastic strain. The equilibrium condition for structurally and chemically nonuniform systems thus becomes

$$\Delta\mu(\mathbf{r}) = \Delta\bar{\mu}(\mathbf{r},c) - \kappa\nabla^2 c - \frac{1}{N_\nu}\nabla(N_\nu\kappa)\nabla c + \beta^{el}(\mathbf{r},c) = \Delta\mu_\infty \qquad [5]$$

where $\Delta\mu = \mu_B - \mu_A$ and $\Delta\bar{\mu} = \bar{\mu}_B - \bar{\mu}_A$, κ is the gradient-energy coefficient, N_ν is the number of atomic sites per unit volume, and $\beta^{el}(\mathbf{r},c)$ accounts for the contribution from the coherency strain energy associated with concentration nonuniformity. The coherency strain energy is measured from a reference state of identical concentration nonuniformity but with each volume element of uniform composition separated into stress-free portions. Different from a structurally uniform system, κ and N_ν are functions of position because of the presence of dislocations.

As mentioned previously, the long-range elastic interaction between lattice distortions caused by a misfitting solute and by a dislocation draws solute atoms toward or away from dislocations, forming a Cottrell atmosphere. In the meantime, any concentration nonuniformity produces a coherency strain in the crystal lattice because of the composition-dependent lattice parameter. To characterize quantitatively the contributions to the total free energy from these elastic interactions, one needs to formulate the elastic strain energy as a function of arbitrary dislocation characters and configurations as well as solute types and distributions. The theoretical treatment of such an elasticity problem was developed by Khachaturyan and Shatalov (KS)[46–48] who derived a close form of the elastic strain energy for arbitrary compositional and structural nonuniformities in an elastically anisotropic crystal under the homogeneous modulus assumption. According to the microelasticity theory of KS,[46] one can solve the mechanical equilibrium equation with an arbitrary stress-free transformation strain or eigenstrain in three dimensions using Green's function, which yields[46,49,50]

$$E^{el} = \frac{1}{2}\sum_{\mathrm{p,q}}\int\frac{d\mathbf{g}}{(2\pi)^3}B_{pq}(\mathbf{e})\tilde{\phi}_p(\mathbf{g})\tilde{\phi}_q^*(\mathbf{g}) \qquad [6]$$

where $\tilde{\phi}_p(\mathbf{g})$ is the Fourier transform of the function $\phi_p(\mathbf{r})$ that characterizes arbitrary compositional or structural

nonuniformities; **r** and **g** represent an arbitrary point in the real and reciprocal space, respectively; * indicates complex conjugate; and **e** = **g**/g.

$$B_{pq}(\mathbf{e}) \equiv C_{ijkl}\varepsilon^0_{ij}(p)\varepsilon^0_{kl}(q) - e_i\sigma^0_{ij}(p)\Omega_{jk}(\mathbf{e})\sigma^0_{kl}(q)e_l \qquad [7]$$

where C_{ijkl} are the elastic constants, $\varepsilon^0_{ij}(p)$ is the stress-free strain of type p inhomogeneity, $\sigma^0_{ij}(p) \equiv C_{ijkl}\varepsilon^0_{kl}(p)$, and $\Omega^{-1}_{jk}(\mathbf{e}) = C_{ijkl}e_ie_l$ is the inverse of Green's function in the reciprocal space $\oint$ in Eq. (6) represents the principle value of the integral that excludes a small volume in the reciprocal space, $(2\pi)^3/V$, at $\mathbf{g} = 0$ (V is the total volume of the system). Detailed examples can be found in the monograph by Khachaturyan.[46]

Equation [6] has been applied successfully to the studies of dislocation-impurity, dislocation-precipitate, and dislocation-dislocation interactions.[21–24,34,37,39,42,43,51,52] When p and q indicate dislocations, Eq. (6) characterizes the self- and interaction energy of dislocations, with p and q indexing individual slip systems consisting of slip plane α and slip direction m_α on that plane, *e.g.*, $\phi_p(\mathbf{r}) = \eta(\alpha,m_\alpha,\mathbf{r})$. $\eta(\alpha,m_\alpha,\mathbf{r})$ is a nonconserved field that characterizes the spatial distribution of an arbitrary configuration of dislocations of slip system (α,m_α).[21–24] Correspondingly,

$$\varepsilon^0_{ij}(p) = \frac{1}{2d}[b_i(\alpha,m_\alpha)n_j(\alpha) + b_j(\alpha,m_\alpha)n_i(\alpha)] \qquad [8]$$

where **n** is the slip plane normal, **b** is the Burger's vector, and d is the interplanar spacing of the slip planes. When p and q represent concentration inhomogeneity, Eq. (6) describes the coherency strain energy, with $\phi_p(\mathbf{r}) = c(\mathbf{r}) - c_\infty$ and $\varepsilon^0_{ij}(p)$ being the stress-free strain associated with the p-type concentration nonuniformity measured from a reference state of uniform concentration of c_∞. Finally, when p and q indicate the concentration nonuniformity and dislocation, respectively, Eq. (6) characterizes the dislocation-solute interactions.

Using such a formulation of the elastic strain energy, the contributions to the exchange chemical potential from the elastic interactions between solute atoms and dislocations and from the coherency strain attributable to concentration nonuniformity can be described self-consistently by

$$U^{el}_B(\mathbf{r}) - U^{el}_A(\mathbf{r}) + \beta^{el}(\mathbf{r},c) = \frac{1}{N_V}\frac{\delta E^{el}}{\delta c} \qquad [9]$$

Substituting Eqs. (1) through (4) and Eq. (9) into Eq. (5) yields the equilibrium solute concentration at an arbitrary configuration of dislocations

$$\frac{c}{1-c} = \frac{c_\infty}{1-c_\infty}\exp\left(-\frac{\Delta F^{seg}}{k_BT}\right) \qquad [10]$$

where the free energy of segregation is given by

$$\Delta F^{seg} = \bar{\mu}^{xs}(\infty,c) - \bar{\mu}^{xs}(\infty,c_\infty) + U^{ch}(\mathbf{r}) + \varphi(c,\mathbf{r}) + \frac{1}{N_V}\frac{\delta E_{el}}{\delta c} - \kappa\nabla^2 c - \frac{1}{N_V}\nabla(N_V\kappa)\nabla c \qquad [11]$$

and $U^{ch} = U^{ch}_B - U^{ch}_A$ and $\varphi = \varphi_B - \varphi_A$. The excess dislocation line energy (the line energy difference between dislocations in a system of arbitrary concentration nonuniformity and a system of uniform concentration of c_∞) is given by

$$E = \iint N_V\{c(\bar{\mu}_B - \bar{\mu}^\infty_B) + (1-c)(\bar{\mu}_A - \bar{\mu}^\infty_A) + \frac{\kappa}{2}(\nabla c)^2 + E_{el}\}dA \qquad [12]$$

Different formulations of the stress-free strain, $\varepsilon^0_{ij}(p)$, for dislocation were used by Hu and Chen[37] and Hu *et al.*[39] in Eq. (7) to study solute segregation. Although a regular solution model was used in these studies, the short-range solute-dislocation core interaction and spatial variation of the gradient-energy coefficient and the enthalpy of mixing near a dislocation were ignored.

B. *Diffusion and Migration*

For a moving dislocation, the flux of solutes in a reference frame moving with the dislocation at a velocity, **v**, is given by

$$\mathbf{J} = -N_Vc(1-c)\left[(1-c)\frac{D_A}{k_BT} + c\frac{D_B}{k_BT}\right]\nabla(\mu_B-\mu_A) - N_Vc\mathbf{v} \qquad [13]$$

where D_A and D_B are the self-diffusivities of solvent and solute atoms, respectively, which are assumed to be equal in this study (*i.e.*, $D_\mathrm{A} = D_\mathrm{B} = D$). The corresponding solute concentration profile around a moving dislocation is then given by

$$N_\nu\frac{\partial c}{\partial t} = -div\mathbf{J} \qquad [14]$$

The steady-state drag force by solute atoms on dislocation gliding along the ξ coordinate can be determined by the energy dissipation method of Hillert and Sundman[14]

$$P_s = -\frac{1}{v}\int_{-\infty}^{\infty}\mathbf{J}_\xi\cdot\frac{d(\mu_B-\mu_A)}{d\xi}d\xi \qquad [15]$$

III. MODEL SYSTEM

This analysis of impurity segregation at dislocations is quite general, independent of any assumptions about a particular dislocation configuration, solid solution model, atom-dislocation interaction potential, or lattice distortion caused by the atomic size mismatch between the solute and solvent atoms (*e.g.*, dilatational or nondilatational). It is applicable to elastically anisotropic systems with concentration-independent elastic constants. To apply the analysis to a given system, however, one needs to specify a dislocation configuration, a solution model for the chemical

and elastic interactions, and a dislocation core structure. For simplicity, we consider an infinitely long straight edge dislocation (along the z direction in a Cartesian coordinate system) in a cubic binary substitutional alloy of an fcc structure. We assume that the chemical free energy of the alloy can be approximated by a regular solution model with nearest neighbor interactions. Then according to Ma *et al.*[20]

$$\Delta\bar{\mu}^{xs}(\infty,c) - \Delta\bar{\mu}^{xs}(\infty,c_\infty) = 2Z_\infty\omega(c_\infty - c) \qquad [16]$$

$$\varphi(c,x,y) = \Delta Z(x,y)\omega(1-2c) \qquad [17]$$

$$U^{ch}(x,y) = \Delta Z(x,y)\frac{\omega_{BB}-\omega_{AA}}{2} \qquad [18]$$

$$\kappa(x,y) = 2\omega d_0^2 Z(x,y) \qquad [19]$$

where $\Delta\bar{\mu}^{xs} = \bar{\mu}_B^{xs} - \bar{\mu}_A^{xs}$, Z_∞ is the coordination number of atoms in a perfect crystal; $\omega = \omega_{AB} - (\omega_{AA} + \omega_{BB})/2$ is the mixing energy; ω_{ij} is the bonding energy between atoms i and j; $\Delta Z(x,y) = Z(x,y) - Z_\infty$, where $Z(x,y)$ is the effective coordination number of atoms in the dislocation core region, which varies in the (x,y) plan only; and d_0 is the interplanar distance of the {111} planes. Correspondingly, the segregation energy becomes

$$\Delta F^{seg} = 2\Omega(c_\infty - c) + \Delta Z(x,y)\frac{\omega_{BB}-\omega_{AA}}{2} + \Delta Z(x,y)\omega(1-2c) + \frac{1}{N_V}\frac{\delta E_{el}}{\delta c} - 2\omega d_0^2 Z(x,y)\nabla^2 c - \frac{2\omega d_0^2}{N_V}\nabla(N_V Z(x,y))\nabla c \qquad [20]$$

with $\Omega = Z_\infty\omega$.

The solute-dislocation interactions within the core consist of two parts: the chemical (or inelastic) interaction associated with missing bonds and the elastic interaction associated with lattice distortion. The elastic interaction is described by the phase field microelasticity model of interactions between structural and concentration nonuniformities described previously. The structural nonuniformity associated with a dislocation is described by the equilibrium profile of $\eta(\alpha,m_\alpha,\mathbf{r})$ obtained from the phase field model of dislocations[21–24] in a chemically uniform system (Figure 1). It is determined by the interplay between the elastic energy and the crystalline energy. The dislocation core structure is characterized by the gradient of $\eta(\alpha,m_\alpha,\mathbf{r})$, which corresponds to the Burger's vector distribution in the Peierls-Nabarro model of dislocations.[2,53,54] It can be seen clearly from Figure 1 that similar to the Peierls-Nobarro model, the phase field model yields a diffuse dislocation core.

To approximate the chemical interaction, we have defined an effective coordination profile, $Z(x,y)$, across the dislocation core in these equations. Without losing generality, we assume a Gaussian function for the profile

$$Z(x,y) = Z(r) = Z_\infty - \Delta Z_m \exp\left(-\frac{r^2}{2w^2}\right) \qquad [21]$$

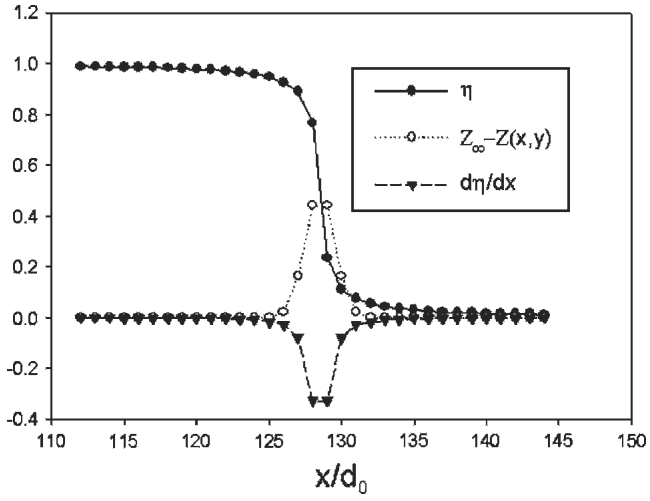

Fig. 1—The equilibrium profiles of η, $\nabla\eta$, and $Z_\infty - Z(x,y)$ across the dislocation core used in the calculations. The equilibrium profile of η is obtained by the phase field model of dislocations.

where $r = \sqrt{x^2+y^2}$, w^2 is the variance of the Gaussian function, and ΔZ_m is the average number of missing bonds per atom along the center of the core. Choosing $w = 1.0d_0$, the effective coordination profile across the dislocation core approximately matches the width of the $\nabla_x\eta$ profile, as shown in Figure 1. The value of ΔZ_m in Eq. (21) is estimated according to the core energy difference between dislocations in pure solvent and pure solute. The current choice of $\Delta Z_m = 0.5$ gives 0.12 eV per atom for this energy difference.

In the elastic energy calculation, we further assume that the lattice parameter of the solution as a function of concentration follows the Vegard law $\left(i.e., \varepsilon_{ij}^{00} = \frac{1}{a}\frac{da}{dc}\delta_{ij}\right)$, where a is the lattice parameter of the host lattice at a stress-free state and δ_{ij} is the Kronecker delta. Although the elastic energy (Eqs. (6) and (7)) is formulated for elastically anisotropic systems, the current study uses only isotropic elastic constants ($\mu = 5.46 \times 10^{10}$ Pa and $\nu = 0.324$) as the Voigt average of the corresponding anisotropic elastic constants: $c_{11} = 16.84$, $c_{12} = 12.14$, and $c_{44} = 7.54 \times 10^{10}$ Pa.[2] The effect of elastic anisotropy on segregation will be investigated in a separate paper.

The remaining material constants used in the calculations are $a_A = 0.361$ nm, $a_B = 0.408$ nm, $d_0 = a_A/\sqrt{3}$, $Z_\infty = 12$, $\omega = 49.7$ meV, and $\omega_{BB} - \omega_{AA} = 0.09$ *eV*. The two-dimensional computational cell (Figure 2) consists of a pair of infinitely long straight edge dislocations (along the z dimension) of opposite signs, one at the center and the other at the boundary. The reason for the choice of such a configuration is for the convenience of carrying out the simulations using a periodic boundary condition. With the periodic boundary condition applied along the x and y directions, the system contains a periodic array of dislocations rather than a single dislocation in an infinite crystal. The system size used in the simulations is 256×256. Increasing the system size to 512×512 does not produce any significant difference in the segregation profiles, as shown in Figure 3, which indicates that the effect from the dislocation-dislocation interaction on segregation can be neglected.

IV. RESULTS AND DISCUSSION

For a system with positive mixing energy ($\omega > 0$), phase separation is expected when alloy composition and temperature are within the miscibility gap. If extended crystalline defects exist, however, wetting transition of solutes at these defects has been predicted[1,17,18,20,55,56] when the bulk alloy composition is outside the miscibility gap. We now explore this segregation transition, together with the conventional segregation at dislocations, using the approach and model system discussed previously.

A. *Stationary Dislocation*

We start with a system of uniform concentration, c_∞, and perform a series of calculations on cooling and heating at temperatures in the single-phase region of the bulk-phase diagram. The equilibrium solute concentration around the dislocations at each temperature is obtained by solving Eq. (10) using the conventional iteration method, with the equilibrium concentration profiles obtained at previous temperatures serving as the initial conditions of new calculations. The simulations are terminated when the concentration profile converges to a stationary value.

Figure 4 shows the contours of the equilibrium solute concentration profiles around the dislocation calculated at

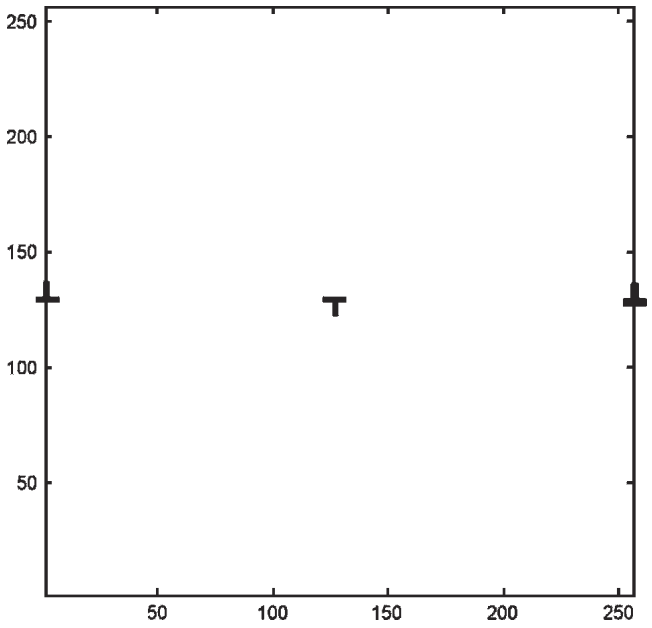

Fig. 2—Schematic drawing of the computational cell.

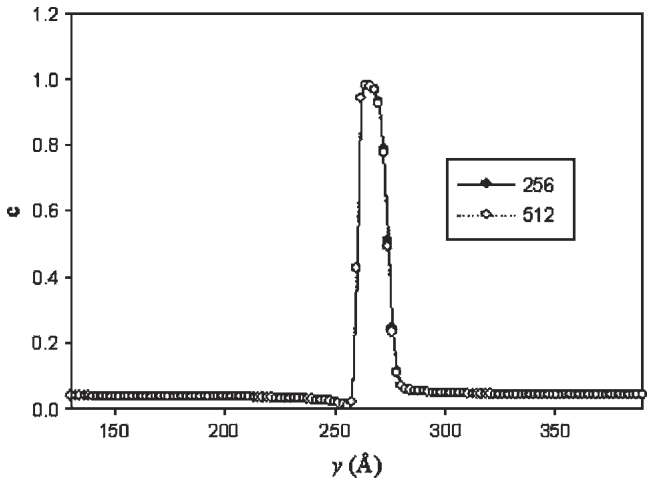

Fig. 3—Comparison between solute concentration profiles along a vertical line through the center of the dislocation core obtained using 256 × 256 and 512 × 512 system sizes.

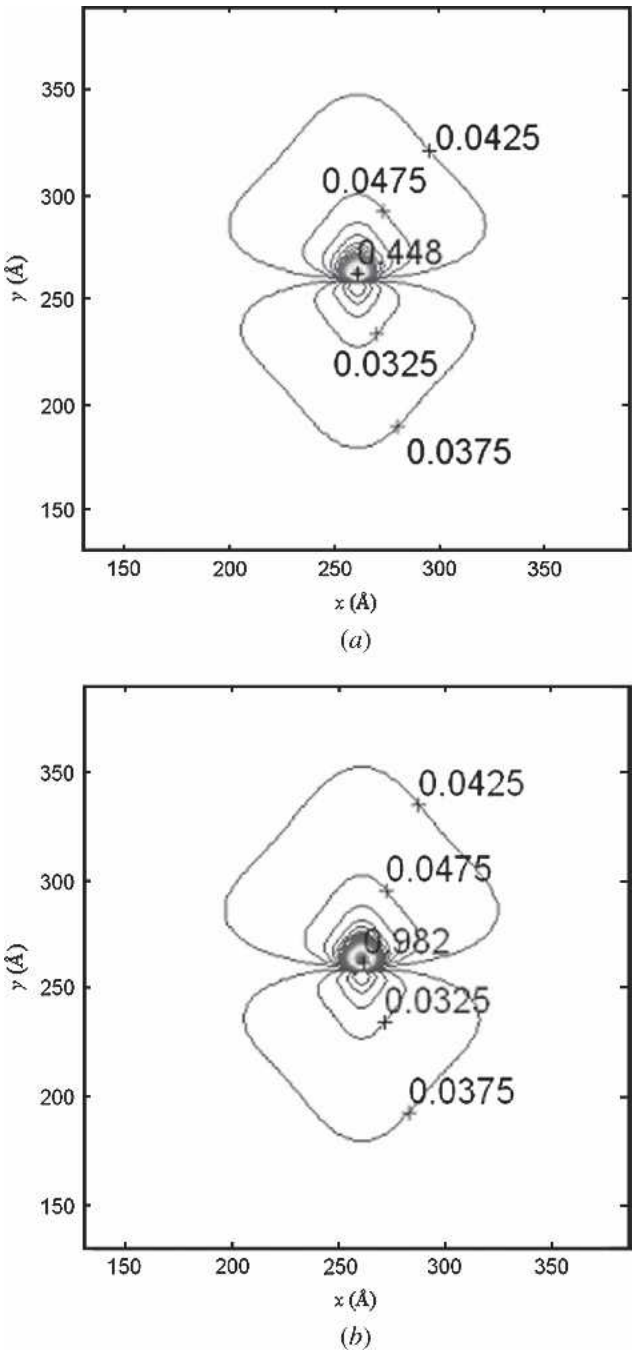

Fig. 4—Contour plots of solute concentration around the dislocation at 1200 K (above the segregation transition T_0) (*a*) and 1170 K (below T_0) (*b*) with bulk composition $c_\infty = 0.04$.

two temperatures (1200 K and 1170 K) above the bulk miscibility gap for an alloy of $c_\infty = 0.04$. The one-dimensional concentration profiles along a vertical line across the center of the dislocation core are shown in Figure 5. Clearly, heavy segregation is confined within the core region at both temperatures. At 1200 K (Figures 4(a) and 5(a)), the peak solute concentration reaches 0.448, which is more than 10 times of the bulk solute concentration. It is, however, still far from saturation (unity). These results are qualitatively similar to the predictions made using the Monte Carlo simulations[38] and the phase field simulations.[39,43] When the temperature is lowered by just 30 K (still above the bulk miscibility gap in the single-phase region), the solute concentration at the core region jumps to 0.982 (close to saturation) (Figures 4(b) and 5(b)). At the same time, the segregation peak becomes much broader and the concentration profile resembles a new phase particle. This indicates that a wetting transition has taken place.

To examine the wetting transition behavior further, we calculate the relative Gibbs excess of solute, Γ_B, and the excess dislocation line energy as functions of temperature on heating and cooling for the alloy. The relative solute excess is calculated according to

$$\Gamma_B = \frac{N_V d_0^2}{1 - c_\infty} \sum_{i,j} [c(i,j) - c_\infty] \qquad [22]$$

and the excess dislocation line energy is calculated using Eq. (12). The results are shown in Figure 6. There are two remarkable features about the variation of the solute excess with temperature at the dislocation core. First, in contrast to the conventional prediction that continuous changes in temperature lead to continuous changes in the amount of segregating solutes, rather abrupt changes in the solute excess (*i.e.*, wetting-nonwetting transitions) are observed at certain temperatures. Second, the transition occurs at different temperatures on heating and cooling, leading to a hysteresis loop. This indicates that the wetting transition at dislocation is a first-order phase transition. The actual transition temperature (T_0) is indicated by the vertical thick line within the hysteresis loop, which is determined by the criterion that the line energy of the dislocation of low segregation

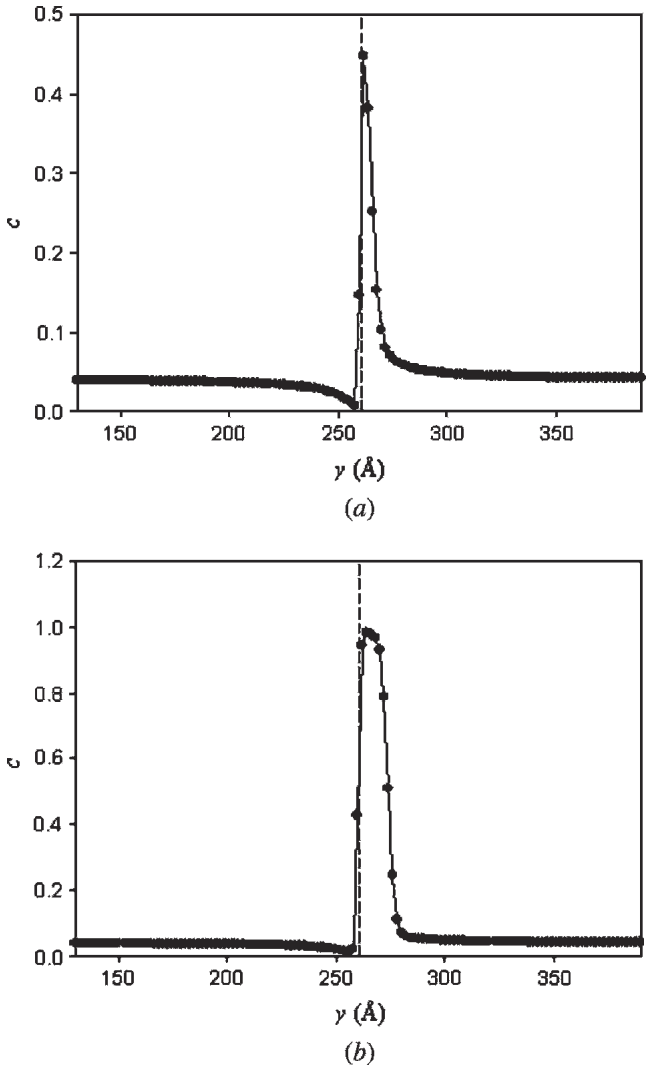

Fig. 5—Solute concentration profile along a vertical line through the center of the dislocation core at 1200 K (*a*) and 1170 K (*b*). The dashed lines in the plots indicate the center of the dislocation core.

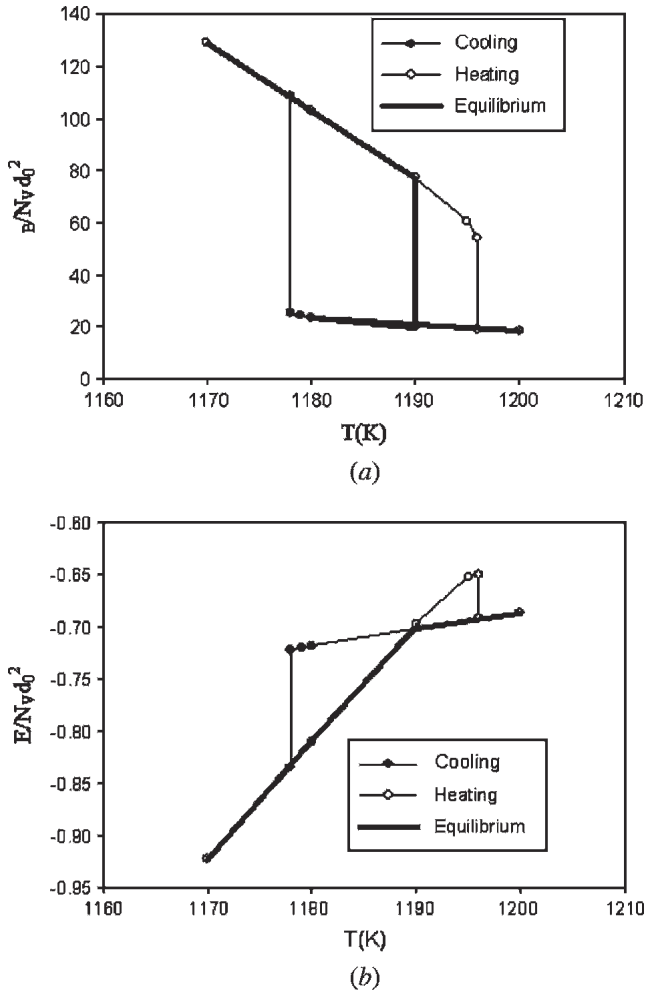

Fig. 6—Variations of a relative Gibbs excess of solute at the dislocation (*a*) and excess dislocation line energy (*b*) as functions of temperature during cooling (solid circles) and heating (open triangles) in a system of bulk composition $c_\infty = 0.04$. The thick vertical line in (*a*) indicates the equilibrium segregation transition temperature.

equals that of high segregation at the transition temperature (Figure 6(b)).[20]

The transition temperatures for alloys of different compositions are plotted in Figure 7(a), along with the bulk miscibility gap. For comparison, the transition temperatures and bulk miscibility gap calculated for an incoherent system (without considering the coherency strain energy in the model) are also presented in Figure 7(a). It can be seen that the coherency strain energy suppresses the bulk miscibility gap and the wetting transition temperatures. In both cases, however, the wetting transition occurs at temperatures significantly higher than the bulk miscibility gap. For the coherent system, the wetting transition ends at $c_\infty \sim 0.056$, where the sharp transition between the high and low segregation as well as the hysteresis loop disappears, whereas the transition ends at a higher bulk concentration in the incoherent system. A more careful comparison is made in Figure 7(b) by plotting the normalized miscibility gaps and wetting transition curves (by the bulk critical temperatures) in the same diagram. The normalized miscibility gaps become identical for the coherent and incoherent systems. It becomes clear that the coherent wetting transition has a wider temperature range between the bulk miscibility gap and the wetting transition curve at the same bulk concentration, c_∞, as compared to the incoherent wetting transition. Qualitatively, this is not difficult to understand, because incorporation of the coherency strain energy is equivalent to reducing the regular solution constant, Ω, which suppresses the bulk miscibility gap as well as the segregation transition temperature. In addition to those terms that contain ω in the segregation energy (Eq. (20)), however, there are other terms that are independent of ω. Therefore, it is anticipated that the change of the regular solution constant may not affect the bulk miscibility gap and the segregation transition to the same extent.

B. *Moving Dislocation*

In contrast to the stationary dislocation, solute concentration around a moving dislocation in the steady-state regimen is determined by solving the continuity equation (Eq. (14)) using the same dislocation configuration as shown in Figure 2. To be self-consistent with the calculations carried out for the stationary dislocation using the iteration method, where the change of the solute concentration profile at the dislocation does not affect the bulk concentration, c_∞, the system is attached to a reservoir of fixed bulk concentration, c_∞. When the velocity is set to zero, the simulation results converge to those obtained using the iteration method.

The simulations are started with an equilibrium solute concentration above the transition temperature determined for a stationary dislocation. We then assume that the dislocation moves at a constant velocity at this temperature and calculate the concentration profile around it. After a system has reached a steady state, the solute concentration profile is used as the initial condition of a new calculation with a different velocity. Figure 8 shows the contour plots of the solute concentration at the dislocation obtained at different velocities. The solute atmosphere becomes asymmetric, with a greater portion trailing behind the moving dislocation. As the velocity increases, the size and the peak concentration of the atmosphere decrease and the degree of asymmetry increases (*e.g.*, the atmosphere elongates in the opposite direction of the dislocation motion and contracts along the direction that is perpendicular to the moving direction).

The plots of the relative Gibbs excess of solute and the drag force as a function of velocity obtained from the simulations are shown in Figure 9. It is found that the Gibbs excess of solute around the dislocation decreases gradually as the dislocation velocity increases (Figure 9(a)). The drag force first increases with increasing dislocation velocity at small velocities and then decreases with increasing velocity at large velocities (Figure 9(b)). In both plots, the variations are smooth, indicating a gradual breakaway of the solute atmosphere from a moving dislocation.

When the temperature is below the wetting transition temperature but above the bulk miscibility gap, however, abrupt changes in solute concentration (Figure 10), relative Gibbs excess, and drag force (Figure 11) occur at certain critical velocities. Qualitatively, the shape changes of the

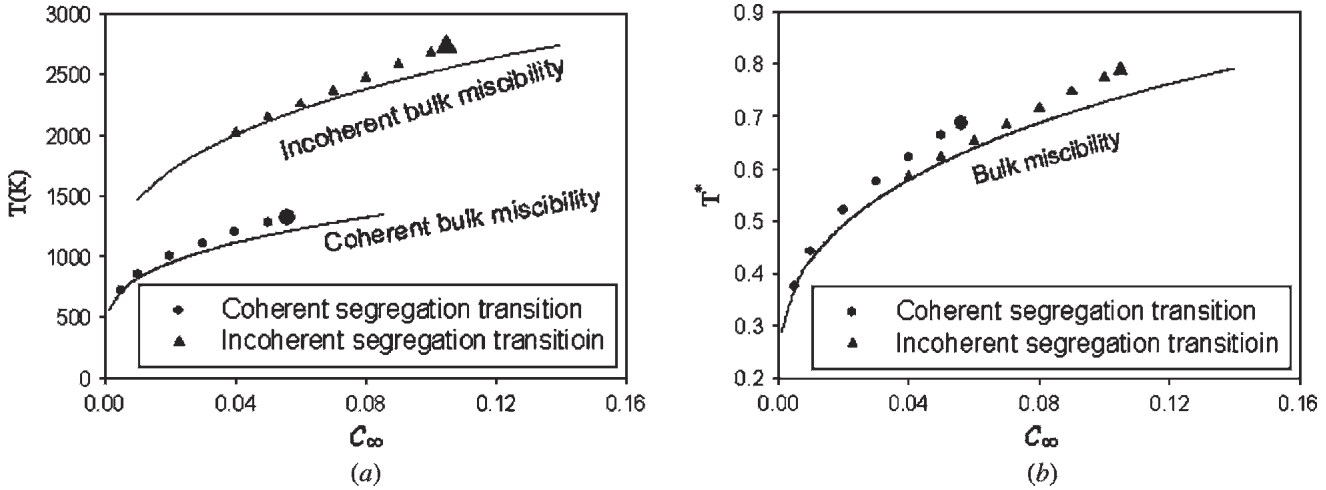

Fig. 7—(*a*) Stability diagrams for segregation transition at dislocation (solid circles and triangles) and bulk miscibility gaps (solid lines) for coherent and incoherent systems. (*b*) Normalized stability diagrams and bulk miscibility gaps. The normalization factors are the critical temperatures for the bulk miscibility gaps of the coherent and incoherent systems, respectively. After normalization, the two bulk miscibility gaps become identical (solid line in (*b*)).

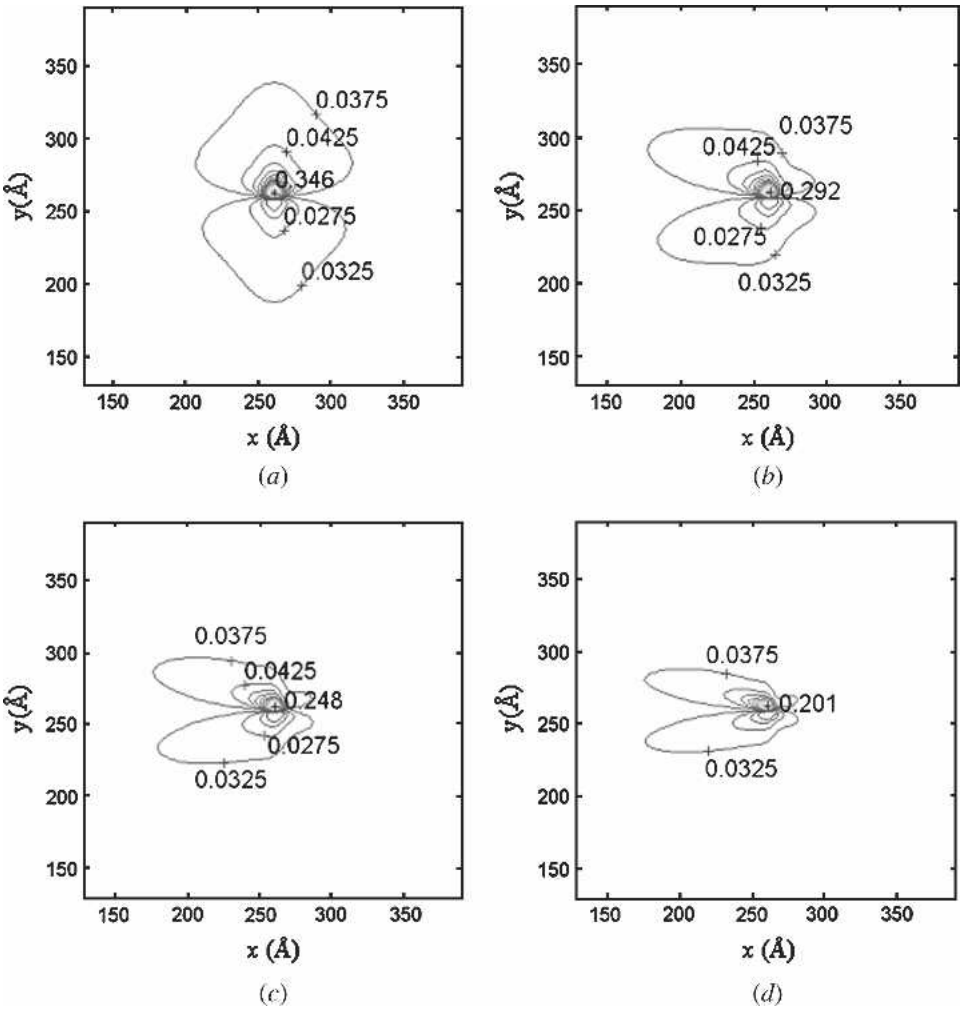

Fig. 8—Contour plots of solute concentration around a moving dislocation at 1200 K (above the segregation transition temperature [T_0]) under various velocities: (*a*) $vd_0/D = 0$, (*b*) $vd_0/D = 1 \times 10^{-3}$, (*c*) $vd_0/D = 2 \times 10^{-3}$, and (*d*) $vd_0/D = 4 \times 10^{-3}$. The bulk composition is $c_\infty = 0.035$.

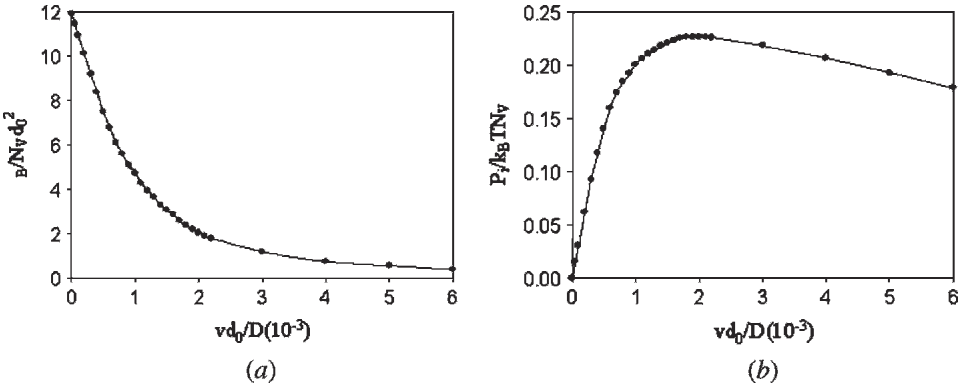

Fig. 9—Variation of Gibbs excess of solute (*a*) and drag force with velocity (*b*) for a moving dislocation at 1200 K (above the segregation transition temperature). The bulk composition is $c_\infty = 0.035$.

solute atmospheres around the moving dislocation as a function of velocity, as shown in Figure 10, are similar to those obtained at a temperature above the wetting transition temperature (Figure 8). The major difference is within the core, where the solute concentration at the center of the core drops sharply (from 0.937 to 0.353) when the velocity exceeds a critical velocity. From Figure 11, one can see clearly that starting from the equilibrium condition at $vd_0/D = 0$, the solute excess at the dislocation decreases and the drag force increases gradually when the velocity

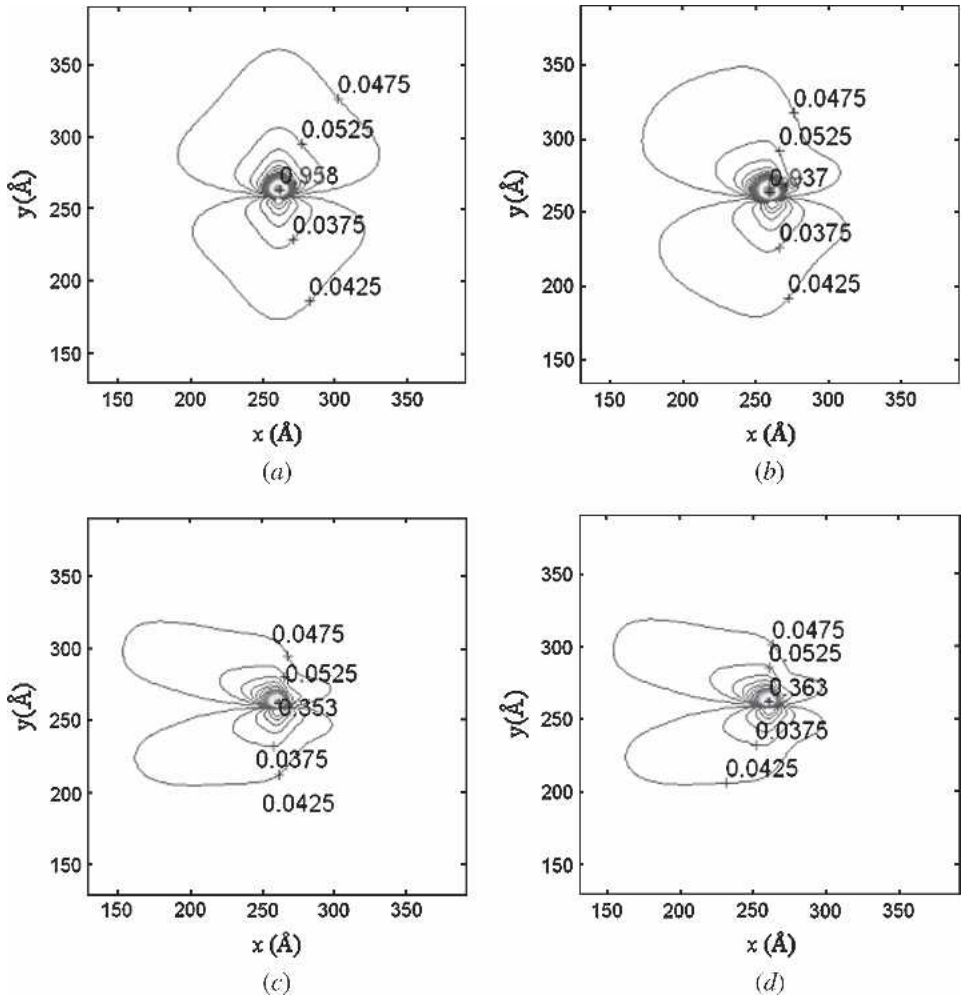

Fig. 10—Contour plots of solute concentration around a moving dislocation at 1200 K (below the segregation transition temperature) with increasing velocities: (*a*) $vd_0/D = 0$, (*b*) $vd_0/D = 0.3 \times 10^{-3}$, (*c*) $vd_0/D = 1 \times 10^{-3}$, and (*d*) $vd_0/D = 2 \times 10^{-3}$. The bulk composition is $c_\infty = 0.045$.

increases. When the velocity reaches a critical value ($vd_0/D \approx 3 \times 10^{-4}$), however, a sharp drop in solute excess and, correspondingly, a sharp drop in the drag force are observed. Although one may refer to the drops as solute breakaway, this phenomenon has a similar nature to the wetting-nonwetting segregation transition taking place at the stationary dislocation with varying temperature. For example, the fundamental characteristics of the variation of the Gibbs excess at the dislocation as a function of dislocation velocity shown in Figure 11(a) are similar to those observed for the stationary dislocation as a function of temperature (Figure 6(a)). In the former, the role of temperature is played by velocity, which, in addition to making the concentration profile asymmetric (along the glide direction), tends to reduce solute segregation at the dislocation. When the dislocation velocity is reduced, an inverse transition occurs but at a lower critical velocity ($vd_0/D \approx 1 \times 10^{-4}$), leading to hysteresis loops in the solute excess versus velocity and the drag force versus velocity plots. Note that the current calculations are performed under constant dislocation velocities rather than under constant applied shear stresses and that the high- and low-segregation and high- and low-drag force branches are different from the high- and low-velocity branches observed under the constant stress condition.[38]

After the transition, further increases in velocity result in further decreases in the maximum solute concentration at the dislocation (Figure 11(b)), and the dislocation experiences a second solute breakaway that is normally referred to in the literature. The two breakaways observed here are similar to that predicted for impurity segregation at migrating grain boundaries.[20] In the case of dislocations, the first breakaway may correspond to the sharp yield point drop and the second breakaway (and resegregation) may correspond to the serration observed on the stress-strain curves of some metal alloys.

In the moving dislocation calculations, we have chosen to change the bulk alloy composition, c_∞ rather than temperature to change the initial state of the system from below to above the wetting transition. The purpose of doing so is to demonstrate that the wetting transition takes place with varying temperature, dislocation velocity, and bulk composition.

These results were obtained for the specific alloys considered. Even though the qualitative characteristics of the segregation transition and the segregation profiles are not

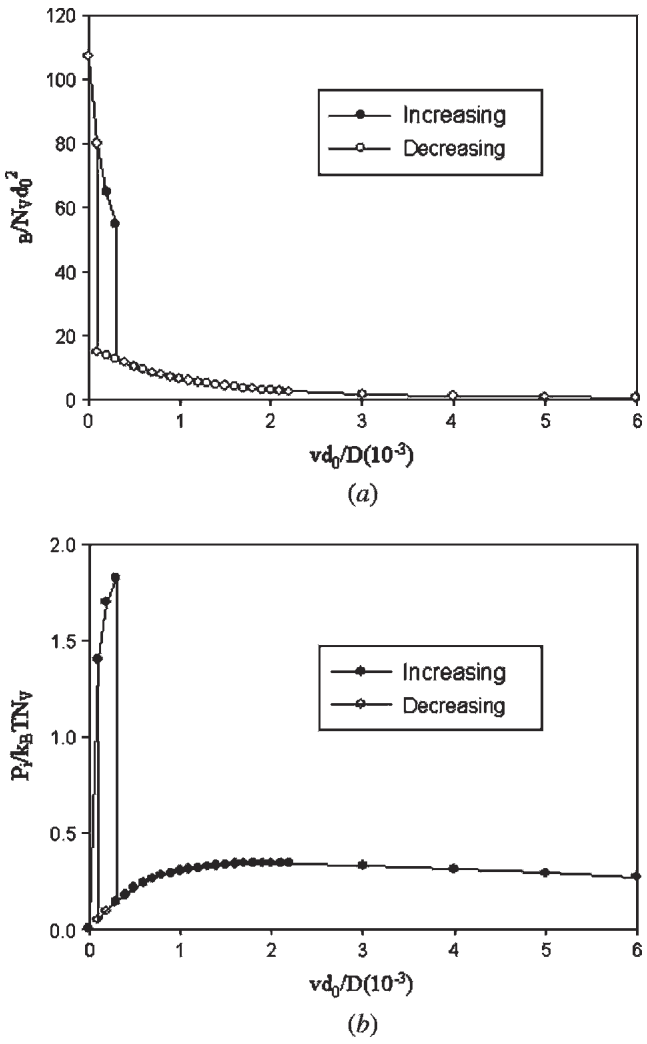

Fig. 11—Variation of Gibbs excess of solute (*a*) and drag force (*b*) with velocity for a moving dislocation at 1200 K (below the segregation transition temperature). The bulk composition is $c_\infty = 0.045$. Solid circles represent values obtained with increasing velocity, whereas open circles represent values obtained with decreasing velocity.

expected to change, the quantitative features of the results alter when different approximations of the solid solution model, dislocation core structure, and solute-dislocation core interactions as well as different material parameters are used. The detailed effect of dislocation core structures as well as the effect of elastic anisotropy and nondilatational misfit strain between solute and solvent atoms will be investigated separately in a forthcoming study.

V. SUMMARY

The chemical equilibrium in a system of stationary and gliding dislocations is analyzed by a continuum model of segregation based on gradient thermodynamics and a phase field model of dislocations. In addition to the long-range elastic solute-dislocation interactions, the analyses take into account several distinct terms accounting for the short-range chemical interactions, concentration gradient, coherence elastic strain, and spatial variation of the gradient-energy coefficient and the enthalpy of mixing near a dislocation. In addition to the well-known phenomenon of formation of the Cottrell atmosphere and its breakaway from a moving dislocation, the application of the model to straight edge dislocations in a regular solution predicts a first-order wetting transition from high to low segregation at the dislocation core with changing temperature, bulk composition, and dislocation velocity. The segregation transition with respect to velocity results in an additional breakaway. This phenomenon could play an important role in determining the deformation behavior of alloys and provide new insights into the sharp yield point drop and the PLC effect.

ACKNOWLEDGMENTS

The authors acknowledge the financial support of the National Science Foundation under DMR-0080766 and the U.S. Air Force Research Laboratory, Materials and Manufacturing Directorate, under the MAI project (grant no. F33615-99-2-5215). They thank Professor J. Li for many invaluable discussions.

REFERENCES

1. A.P. Sutton and R.W. Balluffi: *Interfaces in Crystalline Materials,* Oxford Science Publications, Clarendon Press, Oxford, England, 1995.
2. J.P. Hirth and J. Lothe: *Theory of Dislocations,* 2nd ed., John Wiley & Sons, New York, NY, 1982.
3. J.D. Ven der Waals: *Konink. Akad. Weten. Amsterdam, Sec. 1,* 1893, vol. 1, p. 8. English translation (with commentary): J.S. Rowlinson: *J. Stat. Phys.,* 1979, vol. 20, pp. 197-200.
4. L.D. Landau: *Sov. Phys. JETP,* 1937, vol. 7, p. 19.
5. E.M. Lifshitz: *Sov. Phys. JETP,* 1941, vol. 11, p. 269.
6. A. Einstein: *Ann. d. Physik,* 1910, vol. 33, p. 1275.
7. L.S. Ornstein and F. Zernicke: *Proc. Acad. Sci. Amst.,* 1914, vol. 17, pp. 793-806.
8. M.A. Krivoglaz and A.A. Smirnov: *Theory of Ordering Alloys,* State Publishing House for Physical and Mathematical Science, Moscow, U.S.S.R., 1958.
9. J.W. Cahn and J.E. Hilliard: *J. Chem. Phys.,* 1958, vol. 28, pp. 258-67.
10. S. Ono: *Mem. Fac. Eng. Kyushu Univ.,* 1947, vol. 10, p. 195.
11. M. Hillert: D.Sc. Thesis, Massachusetts Institute of Technology, Boston, MA, 1956.
12. M. Hillert: *Acta Metall.,* 1961, vol. 9, pp. 525-35.
13. T. Ericsson: *Acta Metall.,* 1966, vol. 14, pp. 1073-84.
14. M. Hillert and B. Sundman: *Acta Metall.,* 1976, vol. 24, pp. 731-43.
15. P. Wynblatt and R.C. Ku: *Surf. Sci.,* 1977, vol. 65, pp. 511-31.
16. Y.W. Lee and H.I. Aaronson: *Surf. Sci.,* 1980, vol. 95, pp. 227–44.
17. S.A. Dregia and P. Wynblatt: *Acta Metall.,* 1991, vol. 39, pp. 771-78.
18. P. Wynblatt and Y.S. Liu: *J. Vac. Sci. Technol., A,* 1992, vol. 10, pp. 2709-17.
19. P. Wynblatt, A. Saúl, and D. Chatain: *Acta Metall.,* 1998, vol. 46, pp. 2337-47.
20. N. Ma, S.A. Dregia, and Y. Wang: *Acta Mater.,* 2003, vol. 51, pp. 3687-700.
21. Y.U. Wang, Y.M. Jin, A.M. Cuitino, and A.G. Khachaturyan: *Appl. Phys. Lett.,* 2001, vol. 78, pp. 2324-26.
22. Y.U. Wang, Y.M. Jin, A.M. Cuitino, and A.G. Khachaturyan: *Acta Mater.,* 2001, vol. 49, pp. 1847-57.
23. C. Shen and Y. Wang: *Acta Mater.,* 2003, vol. 51, pp. 2595-601.
24. C. Shen and Y. Wang: *Acta Mater.,* 2004, vol. 52, pp. 683-91.
25. A.H. Cottrell: *Report of a Conference on Strength of Solids,* Mott NF, ed., The Physical Society, London, England, 1948.
26. A.H. Cottrell and M.A. Jaswon: *Proc. R. Soc. London, Ser. A,* 1949, vol. 199A, pp. 104-14.
27. A.H. Cottrell and B.A. Bilby: *Proc. Phys. Soc.,* 1949, vol. 62A, pp. 49-62.
28. H. Yoshinage and S. Morozumi: *Philos. Mag.,* 1971, vol. 23, p. 1367.
29. S. Takeuchi and A.S. Argon: *Philos. Mag.,* 1979, vol. 40, pp. 65-75.
30. R. Fuentes-Samaniego and J.P. Hirth: *Phys. Stat. Solidi B,* 1981, vol. 106, pp. 359-71.

31. R. Fuentes-Samaniego, R. Gasca-Neri, and J.P. Hirth: *Philos. Mag.,* 1984, vol. 49, pp. 31-43.
32. R. Fuentes-Samaniego and J.P. Hirth: *Phys. Stat. Solidi B,* 1984, vol. 121, pp. 101-09.
33. A. Portevin and F. Le Chatelier: *C.R. Acad. Sci.,* 1923, vol. 176, pp. 507-10.
34. C. Shen, A. Kazaryan, P.M. Anderson, and Y. Wang: in *Proceedings of the Second International Conference on Computational Nanoscience and Nanotechnology,* M. Laudon and B. Romanowicz, eds., Computational Publications, Cambridge, MA, 2002, pp. 259-62.
35. C.L. Rohrer: *J. Mater. Res.,* 1995, vol. 10, pp. 578-90.
36. R.W. Smith, R. Najafabadi, and D.J. Srolovitz: *Acta Metal. Mater.,* 1995, vol. 43, pp. 3621-32.
37. S.Y. Hu and L.Q. Chen: *Acta Mater.,* 2001, vol. 49, pp. 463-72.
38. Y. Wang, D.J. Srolovitz, J.M. Rickman, and R. Lesar: *Acta Mater.,* 2000, vol. 48, pp. 2163-75.
39. S.Y. Hu, Y.L. Li, Y.X. Zheng, and L.Q. Chen: *Int. J. Plast.,* 2004, vol. 20, pp. 403-25.
40. J.K. Lee: *Metall. Mater. Trans. A,* 1998, vol. 29, pp. 2039-48.
41. F. Leonard and R. Desai: *Phys. Rev. B: Condens. Matter Mater. Phys.,* 1998, vol. 58, pp. 8277-88.
42. D. Rodney and A. Finel: *MRS Symp Proc.,* 2000, vol. 652, Y4.9.1-Y4.9.6.
43. S.Y. Hu and L.Q. Chen: *Comput. Mater. Sci.,* 2002, vol. 23, pp. 270-82.
44. A.N. Guluoglu: *Scr. Mater.,* 1997, vol. 36, pp. 123-28.
45. K.J. Draheim and J. Schlipf: *Comput. Mater. Sci.,* 1996, vol. 5, pp. 67-74.
46. A.G. Khachaturyan: *Theory of Structural Transformations in Solids,* John Wiley & Sons, New York, NY, 1983.
47. A.G. Khachaturyan: *Sov. Phys. Solid State,* 1967, vol. 8, pp. 2163-68.
48. A.G. Khachaturyan and G.A. Shatalov: *Sov. Phys. Solid State,* 1969, vol. 11, p. 118.
49. D.Y. Li and L.Q. Chen: *Acta Mater.,* 1998, vol. 46, pp. 639-49.
50. C. Shen and Y. Wang: in *Handbook of Materials Modeling,* S. Yip, ed., Springer, printed in The Netherlands, 2005, pp. 2117-42.
51. C. Shen, M.J. Mills, and Y. Wang: *MRS Symp. Proc.,* 2003, vol. 753, pp. 309-41.
52. Y.U. Wang, Y.M. Jin, and A.G. Khachaturyan: *Acta Mater.,* 2003, vol. 51, pp. 4209-23.
53. R.E. Peierls: *Proc. Phys. Soc.,* 1940, vol. 52, pp. 34-37.
54. F.R.N. Nobarro: *Proc. Phys. Soc.,* 1947, vol. 59, pp. 256-92.
55. J.W. Cahn: *J. Chem. Phys.,* 1977, vol. 66, pp. 3667-72.
56. C.R. Helms: *Surf. Sci.,* 1977, vol. 69, pp. 689-701.